

Full Length Article

Evolution of the atomic and electronic structures during nitridation of the Si(111) surface under ammonia flux

Vladimir Mansurov^{a,*}, Yury Galitsyn^a, Timur Malin^a, Sergey Teys^a, Denis Milakhin^a, Konstantin Zhuravlev^{a,b}

^a Rzhanov Institute of Semiconductor Physics of Siberian Branch of Russian Academy of Sciences, Novosibirsk 630090, Russia

^b Novosibirsk State University, Novosibirsk 630090, Russia



ARTICLE INFO

Keywords:

Silicon nitride
Graphene-like materials
 π -bonds
Aromaticity
Silicon nitridation
Morphology by STM

ABSTRACT

Evolution of atomic and electronic structures during high temperature Si(111) surface nitridation under ammonia flux was studied in details by the STM/STS techniques. The adsorption and intermediate phases arising at low doses preceding the (8×8) structure formation were determined. Dependence of the STM images contrast on the tunneling gap voltage is interpreted within framework of the WKB tunneling current theory. It is shown that the (8×8) structure is formed over the silicon surface but not in the surface etching pits. Homogeneous disordered high-temperature silicon nitride phase, consisting of $\text{Si}_x\text{N}_y\text{H}_z$ fragments transforms into an inhomogeneous one at phase transition from $(1 \times 1) \rightarrow (7 \times 7)_N$ upon surface cooling. This silicon nitride phase is concentrated mainly in the central areas of the (7×7) DAS structure. A peaks shift in the STS spectra of local electronic states as a function of the ammonia dose is discovered. The nature of the peaks is associated with the electronic states of dangling bonds and/or π -bonds comprising into the $\text{Si}_x\text{N}_y\text{H}_z$ fragments. The $\text{Si}_x\text{N}_y\text{H}_z$ fragments are the building blocks for a graphene-like $g\text{-Si}_3\text{N}_3$ layer with the (8×8) structure. In frame of lattice gas model a lateral interaction of the fragments provides a phase transition to a condensed ordered phase (8×8) .

1. Introduction

1.1. Two-dimensional materials, including two-dimensional silicon nitride

Since two-dimensional (2D) high-quality graphene were prepared by mechanical exfoliation of single layer graphene from highly oriented pyrolytic graphite (HOPG) and its properties were studied, it is considered as the most promising material suitable for the development of the next generation of electronics and nanoelectronics [1]. Attractive in the graphene are its extraordinary electronic properties, namely, the absence of a bandgap, the linear dispersion law. In addition, it has high temperature stability of electronic properties and high thermal conductivity. However, the semimetallic nature of graphene and the absence of a bandgap make it difficult to develop the technology of transistors and switches [2]. To solve such problems and to expand the possible applications of graphene, a number of ideas devoted to the modification (functionalization) of graphene were proposed [3,4]. On the other hand, the discovery of graphene stimulated the search and study of the properties of other 2D crystalline materials with

semiconductor nature. Among them, much attention was attracted to graphite-like carbon-nitride compounds $g\text{-C}_3\text{N}_3$ and $g\text{-C}_3\text{N}_4$. These materials consist of covalently bound sp^2 -hybridized carbon and nitrogen atoms. Interest is caused by theoretical predictions of new mechanical, electronic, magnetic and photocatalytic properties [5–14]. To date, the $g\text{-C}_3\text{N}_4$ compound has been synthesized [14] and it has been demonstrated that the $g\text{-C}_3\text{N}_4$ layers have a bandgap in the range of 1.6–2.0 eV, which makes it possible to use them to create electronic and optoelectronic devices, such as field effect transistors, photodetectors, light-emitting diodes and lasers.

Much less attention was paid to the silicon–nitride compounds with a graphite or graphene structure (such as $g\text{-Si}_3\text{N}_4$, $g\text{-Si}_3\text{N}_3$, etc.), which may have a set of unusual and useful properties. Previously, it was believed that silicon is not capable to form stable aromatic compounds [15]. However, it was recently shown in the works [16–18] that in complex molecules containing cyclic silicon chains, the sp^2 hybridization of atomic orbitals and aromatic bonds occurs. Cyclic Si–N rings, in particular $\text{Si}_3\text{N}_3\text{H}_3$, were considered theoretically in [18], and their stability and aromaticity have been confirmed. In [19], the electronic

* Corresponding author.

E-mail addresses: mansurov@isp.nsc.ru (V. Mansurov), dmilakhin@isp.nsc.ru (D. Milakhin).

<https://doi.org/10.1016/j.apsusc.2021.151276>

Received 2 April 2021; Received in revised form 30 August 2021; Accepted 11 September 2021

Available online 14 September 2021

0169-4332/© 2021 Elsevier B.V. All rights reserved.

and optical properties of the g-Si₃N₃ layer were calculated from the first principles, the bandgap width in this material was theoretically determined by two computational methods: GGA-PBE (2.3 eV) and hybrid functional HSE06 (3.5 eV). However, there are no experimental evidences for the existence of such structures and works devoted to the study of its properties to date. In our recent publications [20,21], we have assumed that (8 × 8) structure, formed on the nitrated silicon substrate surface, consists of aromatic Si₃N₃ rings.

Silicon nitride structures appeared during the Si(111) surface nitridation process were studied in a number of works [22–38]. As a rule, an amorphous phase of silicon nitride is formed during silicon nitridation [29–31], however, at the initial stages of Si(111) surface nitridation at sufficiently high temperatures the ordered (8 × 8) structure was observed [22–25,33–38]. The (8 × 8) structure was discovered for the first time by van Bommel and Meyer in 1967 [33]. This structure and its diverse representations, such as (8/11 × 8/11) and (8/3 × 8/3) structures, have been studied and described later. Let us consider the most important, in our opinion, works. Nishijima and Kobayashi [22–24], as well as Morita [25], investigated the (8 × 8) structure and proposed its atomic model. It was assumed that the (8 × 8) structure is a periodically bent SiN bilayer with a lateral lattice parameter of 2.79 Å on base of sp³ hybridization of the atomic orbitals. In addition, Nishijima and Kobayashi proposed a flat SiN layer model based on sp² hybridized orbitals of silicon and nitrogen atoms, where the silicon and nitrogen atoms are implied tetravalent, which is questionable for nitrogen. Later, the models explaining the (8 × 8) structure on base of thin crystalline layer of β-Si₃N₄ became dominating [34–37]. First, Rottger et al [34] supposed that (8 × 8) structure consists of β-Si₃N₄ structural units. Then Ahn et al [35] proposed a model where the (8 × 8) structure is explained by the formation of a crystalline β-Si₃N₄ monolayer with adsorbed nitrogen atoms on top of it. Later it was proposed to consider the (8 × 8) structure as a reconstruction of the β-Si₃N₄ surface and express this structure on base of the lattice constants of the β-Si₃N₄ phase instead of silicon, that is, denote it as (4 × 4) [36,37].

Earlier, in [20,21,27], we have investigated the (8 × 8) structure formation under exposure of the silicon (111) surface in an ammonia flux at molecular beam epitaxy (MBE) conditions. An ordered structure, consisting of hexagons with a side size of ~ 6 Å, have been experimentally discovered by the scanning tunneling microscopy (STM) technique. Based on this fact and data from reflection high energy diffraction (RHEED), transmission electron microscopy (TEM) and others methods, a model of the (8 × 8) structure have been proposed. According to this model, hexagon consists of 6 Si₃N₃ aromatic rings connected by Si-Si bonds (Fig. 1). Silicon is in sp² hybridization, and nitrogen is in sp-like hybridization, binding in the aromatic ring is carried out by σ- and π-bonds.

Besides, the STM images have demonstrated a periodic adsorption structure (8/3 × 8/3), which we have associated with silicon adatoms [21]. The (8 × 8) structure at elevated temperatures appears due to the interaction of the so-called mobile silicon adatoms with nitrogen. Atomic orbitals of mobile silicon adatoms in this case transform into the sp² configuration with a higher probability than into the sp³ configuration. The formation heat of a mobile silicon adatom on the Si (111) surface as ~ 1.7 eV have been determined [27], that have allowed us to describe the kinetics of (8 × 8) structure formation in agreement with experiment.

1.2. State of research of the initial stages of Si (111) nitridation

1.2.1. Reactivity of corner adatoms, central adatoms and rest-atoms of (7 × 7) structure

The mechanisms of an ordered (8 × 8) superstructure formation are of great interest. In the works of Avouris et al and Wu et al [39–43], the initial stages of Si (111) surface nitridation process with the (7 × 7) reconstruction at the atomic level using STM/STS (scanning tunneling spectroscopy) were investigated. The authors explained the appearance

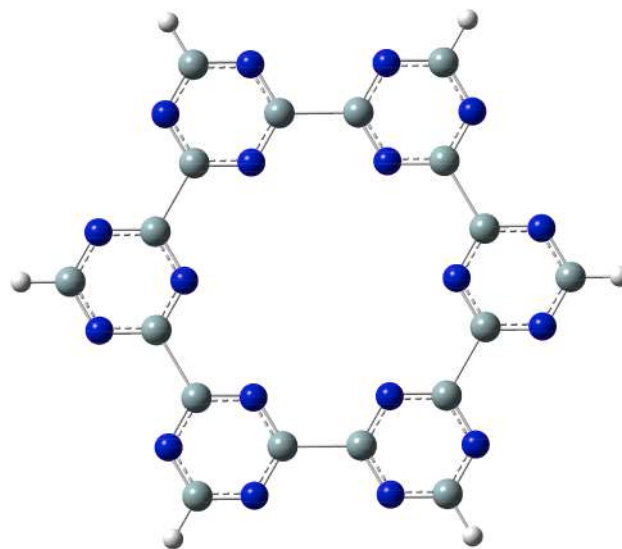


Fig. 1. The fragment of the model of ordered (8 × 8) structure in hexagon form consisted of 6 Si₃N₃ aromatic rings connected by Si-Si bonds, sp² Si-dangling bonds are saturated by hydrogen atoms (dark grey circles denotes Si atoms, blue circles are N atoms, light grey circles are H atoms).

of new contrast as dark areas on this surface during nitridation process by saturation of dangling bonds of (7 × 7) structure with products of dissociative chemisorption of ammonia NH₃ → NH₂ + H, that is, the appearance of single Si-NH₂ and Si-H bonds on the surface. In these works authors believed that the reaction of silicon nitridation with ammonia is not an etching process of the surface. Note that in contrast to this, for example, in the works of Gangopadhaya et al [44,45] and Petrenko et al [46], nitridation and (8 × 8) structure formation are considered as surface etching processes with ammonia. However, these works did not provide unambiguous evidence of surface etching by the reagent.

Actually, the color change (that is, the appearance of dark spots, areas and stripes) in STM images is explained by Avouris et al as the “elimination” of states corresponding to dangling bonds of rest-atoms and/or adatoms on a clean surface. Then, according to Avouris et al, for adatoms, that did not react with ammonia, their color on the images does not change. Unfortunately, the authors of [40] did not provide the STS spectra for the reacted central adatoms, the color change of which predominantly creates the characteristic ordered pattern of the STM for the modified (7 × 7) image after exposure to ammonia; such spectra would make it possible to better understand the evolution of silicon electronic structure under reaction with ammonia.

Note also that the STM images presented by the authors [39–41] contain reacted corner adatoms and unreacted central adatoms. This indicates that any adatoms (both central and corner) can react with ammonia, the difference is only in the ratio of the probabilities of such reactions for a particular adsorption site (or dangling bond). The authors classified adsorption sites of (7 × 7) structure according to their reactivity: dangling bonds of rest-atoms were identified as the most reactive, followed by central adatoms and corner adatoms as the least reactive. Keeping the authors logic and taking into account the experimental observation of reacted corner adatoms, it can be concluded that, in principle, complete filling of the (7 × 7) surface with Si-N and Si-H bonds is possible, that is, saturation of all 19 initial dangling bonds on the (7 × 7) surface with ammonia. For this the dissociative chemisorption of only 10 NH₃ molecules per (7 × 7) cell is sufficient.

In contrast to Avouris et al, Kang [47] based on *ab initio* calculations showed that adatoms are more active under ammonia chemisorption than rest-atoms, and the dangling bonds of rest-atoms are saturated mainly with hydrogen. Also according to this author, dangling bonds of

rest-atoms are completely saturated “earlier” than adatoms, only because in the (7×7) cell there are twice as little. Later, to explain STM images, the “bridging” configuration of Si-NH-Si bonds, which is formed at the site of the back-bond between the adatom and the nearest underlying silicon atom, incorporated in the crystalline bilayer of the substrate, was also considered [48,49].

It is necessary to emphasize the following very important circumstance: it was demonstrated in the work of Wu et al [43] that the use of higher nitrogen doses during low-temperature (for example, room temperature -RT) nitridation process of the silicon surface leads to the formation of an ultrathin nonstoichiometric disordered silicon nitride layer, but (8×8) structure is not formed.

1.2.2. Local electronic structure of the surface

As was established in the works of Wu et al [42,43] and Gangopadhaya et al [44,45], the (8×8) structure can form at elevated temperatures of nitridation process. The appearance of (8×8) structure was manifested itself by the formation of darker regions of triangular (and/or hexagonal) shape in STM images, and it was assumed that (8×8) structure is formed in the etching pits of the silicon surface. However, it is also known that images in scanning tunneling microscopy reflect not only the morphological state of the surface, but also the local electronic structure of the surface, which plays an important role in surfaces species identification and characterization [50,51]. When interpreting STM/STS data, it is necessary to take proper account of the local density of states (LDOS) of the surface, which is usually associated with the differential tunneling conductance $(dI/dV)/(I/V)$. Therefore, the dark areas in the image are not necessarily morphological pits, but may also indicate a decrease in the local density of states (in a certain energy range that was used in the STM/STS measurement) in this area of the surface. Of course, the STM contrast on the clean surface is obviously originate from the morphological contribution, for example, when measuring the height of a step on a clean silicon surface with the same reconstructions on the both terraces.

Despite a large number of studies devoted to nitridation of the Si (111) surface and the formation of the (8×8) structure, the electronic states of this structure have not yet been finally established. For example, in the work of Wu et al [43], the STS spectra of the density of states of (8×8) structure with a bandgap of about 5 eV are demonstrated, and there are no electronic states in the range from -3 to $+2.5$ eV. These results do not agree with the STS data of Flammini et al [52], where the filled electronic states were observed almost from the Fermi level and a pronounced shoulder in the density of states was found near -2.2 eV. Besides, the nitride electronic states at about -2 eV were observed by the authors by angle-resolved photoemission spectroscopy (ARPES). In addition drastically differs from the aforementioned authors results the spectrum of valence states of (8×8) structure obtained by the photoelectron spectroscopy (PES) method by Kim and Yeom [53], where the most intense peak at -1.1 eV was observed. It is interesting to note, that Flammini [52] have prepared the sample by the same method as Kim and Yeom [53], but different electronic spectrum of the (8×8) structure was found.

There is similar situation upon nitridation of the Si (001) surface, on this surface variations in the bandgap on the nitridated surface were also observed in the STS spectra. In the works of Matsushita et al [54–56], at low exposures of the surface in active nitrogen, a small bandgap was observed, while at high exposures the bandgap increased and reached 4 eV. The possibility of the silicon nitride layer formation with a relatively narrow bandgap is also confirmed in the work of Kondo et al [57], where the band width (starting from 0.45 eV on a clean reconstructed Si (001)-(2 × 1) surface) varied from 1.6 to 4.3 eV with varying growth conditions, in particular, the nitridation temperature and the power of nitrogen RF plasma. None of ordered silicon nitride structures were observed in these works.

In our previous works, all experiments on silicon surface nitridation were carried out in an excess of ammonia. In the present work, we

continued the study of nitridation processes under excess silicon conditions. The Si (111) surface nitridation was carried out at high temperatures, depending on the ammonia dose, starting with very low doses, followed by analysis by the STM/STS techniques. This allowed us to study the nitridation evolution and determine which adsorption and intermediate phases arise before and during the (8×8) structure formation. The study of the structure evolution of intermediate phases is combining with investigation of evolution of local electronic states of the surface. The nature of the contrast in STM images is discussed, and on this basis, a comparative analysis of STM/STS images and spectra that was obtained at low and high nitridation temperatures is carried out. The reactivity of various surface species including the DAS (7×7) structure subunits is discussed.

2. Experimental methods

The experiments were carried out independently in two ultrahigh vacuum systems: in a Riber CBE-32P molecular beam epitaxy machine equipped with a RHEED system (12 keV electron gun) and an STM/STS machine. The evolution of the complete diffraction pattern (DP) from the luminescent screen with high cathodoluminescence efficiency was recorded using a kSA-400 system from k-Space Associates Inc., equipped with CCD-based camera and software for recording and analysis of diffraction patterns.

The surface exposure (dose) in ammonia is defined as $D = P \times t$, and was measured in Langmuir (L), where P is the pressure (in our case ammonia), t is the exposure time in ammonia, and according to the definition $1\text{L} = 10^{-6}$ Torr \times 1 s. The nitridation process was studied *in situ* using RHEED technique on insulating silicon substrates Si (111). Surface preparation procedure, formation of a maximal surface coverage with a g-Si₃N₃ layer occurred during exposure of the silicon surface to ammonia in a narrow range of conditions, with an accurate control of the surface temperature, ammonia flux and exposure time, were described in our previous works [20,21,27].

Samples of ultrathin silicon nitride for studies by scanning tunneling microscopy/spectroscopy (STM/STS) were prepared on a conducting n-type Si (111) substrate with a resistivity of $0.3 \Omega \times \text{cm}$ in an ultrahigh-vacuum machine for AFM/STM/STS analysis (Omicron, Germany). This machine is equipped with an ultra-high purity ammonia feed unit and a reflection high-energy electron diffraction system. The preparation of a clean silicon surface for experiments was carried out in two stages. First, the surface was annealed at 600 °C in a preparation chamber for 2 h. Finally, the silicon surface was cleaned at 1250 °C for 30 s. The atomic purity of the Si surface was confirmed by the registration of the (7×7) superstructure. STM images and STS spectra were recorded at room temperature in the constant tunneling current mode, as well as in the current-imaging-tunneling spectroscopy (CITS) mode [58] using an electrochemically sharpened tungsten tip. Typical currents did not exceed 0.1nA (the typical tunneling current used was 0.025nA), and a bias voltage (V_{bias}) relative to the probe potential was applied to the silicon sample in the ± 5 V range. The dependence of the differential conductance $(dI/dV_{\text{bias}})/(I/V_{\text{bias}})$ on the voltage in the tunnel gap (V_{bias}) was determined by numerical differentiation of the measured I - V dependences.

The initial surface for further studies of the nitridation process is a clean Si (111) surface with (7×7) reconstruction. Both machines (MBE and STM) make it possible to reproducibly obtain a clean silicon Si (111) surface, which is confirmed by (7×7) reconstruction images in both RHEED and STM, which are in good agreement with those known in the literature. Calibration of STM measurements of surface morphological features was performed using a monolayer step on a clean silicon (111) surface with (7×7) reconstruction, since this value is well known $- 3.14 \text{ \AA}$. Without normalization, the height of monolayer steps measured on different samples and at three different voltages turned out to be about 4.2 \AA , and the correction factor for the measured heights in our case is $3.14 \text{ \AA}/4.2 \text{ \AA} \approx 0.75$. The height profiles normalized to this

factor for several measurements of steps are shown in Fig. 2.

3. Experimental results and discussion

3.1. Appearance and evolution of atomic (8×8) structure under silicon Si (111) nitridation

Earlier, our RHEED studies have shown that the brightest diffraction patterns with narrow diffraction spots of the (8×8) structure are obtained at a high temperature of silicon nitridation. The spots intensity evolution of this structure during nitridation process demonstrates a maximum at a certain exposure, after which the pattern gradually fades out [27]. More detailed information on the evolution of the structure and electronic states in the silicon nitridation process can be obtained by microscopic studies using STM/STS techniques (see [supplementary materials Part 1](#): comparison of RHEED kinetic curves areas and corresponding STM images).

3.1.1. Evolution of the (7×7)_N nitride structure on the surface before the appearance of (8×8) structure

Fig. 3 shows STM images of a Si surface after small doses (no more than 5L) of ammonia exposure at a temperature of 1000 °C. In what follows, we will use terms that are often encountered in the literature, for example, in [59] when describing individual subunits of the (7×7)-DAS structure, such as “corner adatom” or “central adatom” and others. STM images were obtained at a bias on the sample (relative to the probe) + 1 V and contain information about the empty states of the sample surface.

After exposure of the Si surface to ammonia 0.3L, separate dark areas appear in the image (Fig. 3a), which are comparable in size to the area occupied by one or two adjacent adatoms of the DAS structure. Such dark areas occupy about 3% of the image area (S_{dark}) covered by a structure with the (7×7) periodicity (let us designate this area as $S_{7 \times 7}$), while regular “dark areas” of the DAS structure itself were not taken into account, namely dark corner holes. It is necessary to pay special attention to the fact that under ammonia exposure at a temperature $T = 1000$ °C, a (1×1) structure exists on the silicon surface. That means the absence of corner, central adatoms and rest-atoms, dimers, corner holes, stacking faults characteristic for the (7×7) structure, and (7×7) periodicity occurs only during the sample cooling to temperatures below 830 °C, while STM images are recorded after cooling to room temperature. Let us introduce the coverage of the surface with dark areas as $\theta_{\text{dark}} = S_{\text{dark}}/S_{7 \times 7}$, then for the given dose we have $\theta_{\text{dark}} = 0.03$. With an increase in exposure to 1.5L, the number and size of dark areas increases as well as the inhomogeneity of the image (Fig. 3b) and the coverage is

$\theta_{\text{dark}} = 0.19$. At the dose of 5L, a separate areas merged into continuous curved (self-intersecting) dark stripes with a width approximately corresponding to the distance between the nearest corner adatoms (about 10 Å), the degree of surface coverage reached $\theta_{\text{dark}} \approx 0.45$ (Fig. 3c). The implication is that an increase in the exposure of the heated Si surface to ammonia, there is a monotonic increase in the coverage degree of the surface with the (7×7) structure by dark areas.

Let us also pay attention to the fact that the dark stripes are located mainly in the area of the central adatoms and rest-atoms of the DAS structure. Let us designate such a structure as (7×7)_N, where the N index emphasizes that the surface contains nitrogen atoms and differs from the (7×7) structure of a clean Si (111) surface. Such a predominant arrangement of dark stripes on the central adatoms and the presence of light corner adatoms surrounding the corner holes form a characteristic periodic pattern of dark and light features, with the same periodicity as (7×7) structure, and Fig. 3c well demonstrates such a characteristic ordered pattern. However, the images also show many deviations from an ideal ordering. A thorough analysis of the STM image in Fig. 3c reveals that there are both dark corner adatoms and central adatoms that retained a lighter tone. This indicates that the newly formed (7×7)_N structure is less ordered in comparison with (7×7) DAS structure of pure silicon surface (see [supplementary materials Part 2](#)). Registration of STM images of this surface with a higher resolution did not reveal new features in the region of dark stripes and no other ordered structure, except for the periodicity of the (7×7) structure. In addition, it should be noted that there is no boundary between the structures (7×7)_N and (7×7). This means that the periodic part of the (7×7)_N structure is completely determined by the DAS structure (7×7), and the nitride layer itself does not have its own periodic structure and is located on top of the (7×7) structure (see [supplementary materials Part 3](#)).

With a further dose increasing to more than 5L (and a treatment temperature of 1000C), nuclei of a new ordered (8×8) structure similar to that observed by the authors [44,45] appears on the surface, and the degree of surface coverage with the (7×7)_N structure begins to decrease (if counting from the total surface area), since part of the sample surface is covered by (8×8) structure. In this case, the ratio of the dark and light areas in the images of the (7×7)_N structure itself stops changing, remaining at the $\theta_{\text{dark}} \approx 0.5$ level. According to this fact, we can make a simple estimation of the fraction of the area occupied by the (7×7)_N structure at low exposures, where this structure coexists or is surrounded by a pure (7×7) structure. Based on the proportion occupied by dark areas and assuming $\theta_{(7 \times 7)_N} \approx 2 \times \theta_{\text{dark}}$, it is possible to depict its evolution graphically, as shown in Fig. 4. That is, the dependence reaches its maximum and then a lowering of the $\theta_{(7 \times 7)_N}$ coverage is observed when the exposure is exceeded 4-5L (see [supplementary materials Part 4](#)).

Thus, at the initial stages of nitridation process, both the interaction of silicon atoms with ammonia and the transformation of the initial valence electronic states characteristic for pure silicon on the surface to the state of silicon nitride are manifested in STM images through the additional contrast evolution of the (7×7) structure. Further, more detailed study of such valence states transformation by the STM/STS methods implies the need to take into account at least two aspects: an increase in the ratio of nitrogen atoms with respect to surface silicon atoms, as well as a change in the number of bonds with nitrogen atoms for individual silicon atoms. The possible range of changes in the number of nitrogen neighbors for a silicon atom is from 0 to 4, and at the initial stages of nitridation, the distribution of surface silicon atoms by the number of bonds with nitrogen undergoes a certain evolution until, ultimately, it reaches the composition of Si₃N₄. On the other hand, from scanning tunneling microscopy analysis, the contrast formed as a result of nitridation process can be associated with both morphological changes on the surface and with a change in the local density of electronic states of the surface due to interaction with ammonia. For example, in [44,45] the contrast have been associated by authors with the surface morphology, but in [40,42] it have been associated with the local density of states. The formation of contrast in STM for the formed

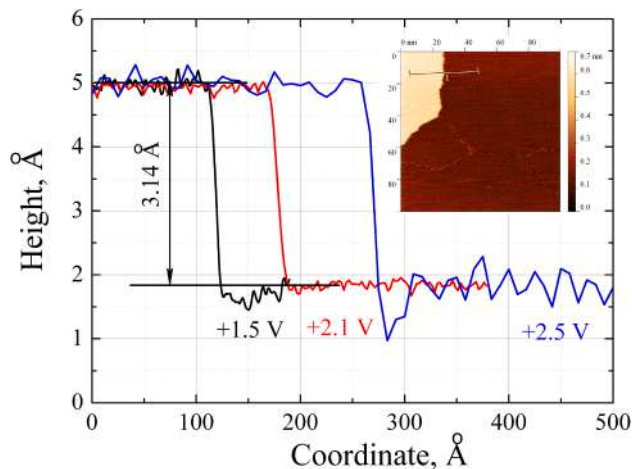


Fig. 2. Normalized height profiles measured at different voltages. Insert: image of a monolayer step on a clean Si (111) surface with (7×7) reconstruction.

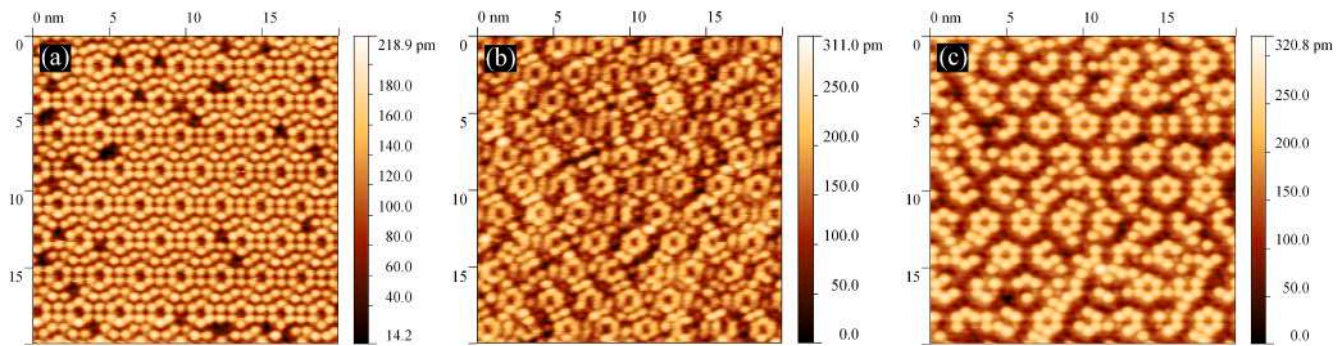


Fig. 3. STM images of the Si (111) surface structure at low doses of sample exposure in ammonia: (a) 0.3L; (b) 1.5L; (c) 5L. Voltage + 1 V, tunneling current 0.025nA.

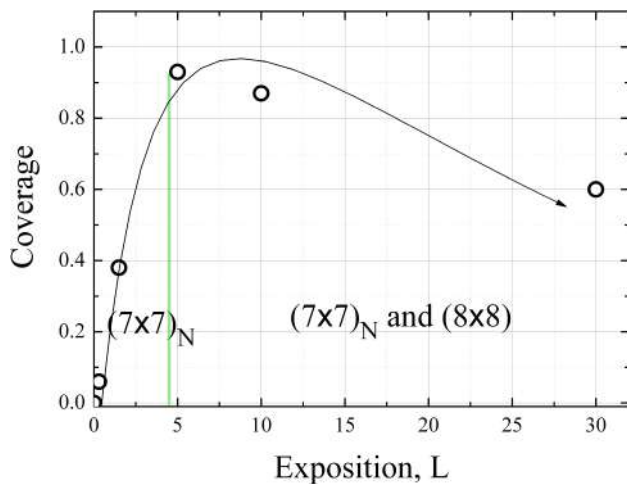


Fig. 4. Dependence of the surface coverage by the $(7 \times 7)_N$ structure on exposure to ammonia.

nitride layer is considered in more details below.

3.1.2. Evolution of (8×8) structure with increasing exposure until the appearance of clusters of amorphous Si_3N_4

Fig. 5 shows images of silicon surfaces treated at 1000 °C with higher ammonia doses in the range 5L – 40L. Regions of a triangular shape are formed on the surface; an examination of these regions with higher resolution revealed a hexagonal (8×8) structure [20,21]. Triangles appear as darker shapes surrounded by light backgrounds. Note that STM images of a light background obtained with a higher resolution demonstrate the same characteristic pattern as in Fig. 3c, that is, these light areas are covered with the $(7 \times 7)_N$ structure. Such kind of contrast with darker shapes is often interpreted as the formation of etching pits [44,45].

It follows from Fig. 5a-d that $(7 \times 7)_N$ and (8×8) structures coexist on the surface in a fairly wide range of surface coverage with silicon nitride. It has been established that an increase in exposure leads to an increase in the degree of surface coverage with a (8×8) structure (see supplementary materials Part 5).

At exposures above 30L new features are revealed in STM images. At Fig. 5d, bright features appear - islands, which we associate with the formation of three-dimensional (3D) clusters of amorphous silicon nitride Si_3N_4 , since earlier STS spectra measured on such kinds of clusters showed a bandgap of more than 5 eV, characteristic of Si_3N_4 [21]. At the same time, it is still possible to find the surface areas covered not only by (8×8) , but also by the $(7 \times 7)_N$ structure. Thus, at an exposure of more than 30 L, the STM images showed the presence of three nitride phases simultaneously: structures $(7 \times 7)_N$ and (8×8) , as well as

clusters of amorphous silicon nitride phase. The evolution of the surface coverage by the (8×8) structure is shown in Fig. 6. The process of (8×8) structure formation terminates at certain value of coverage, despite the fact that the surface is not yet completely covered with this (8×8) structure. Earlier, when studying the nitridation process by the RHEED technique, we have also found that the process of (8×8) structure formation terminates at different coverage levels for various temperatures (including the 1000 °C) [27], see also the comments in the supplementary materials Part 6. The termination of the process was explained by the depletion of the equilibrium concentration of mobile silicon adatoms, since the (8×8) formation process proceeds faster than the restoration of the equilibrium concentration of mobile silicon. Therefore, one can conclude that the dose of ammonia ~ 30 L under these conditions corresponds to the depletion of the mobile silicon concentration.

3.2. Dependence of the STM images contrast as function of the voltage applied to the tunnel gap

During the STM studies of the evolution of $(7 \times 7)_N$ and (8×8) structures, it was found that the operating voltage between the sample and the probe, specified during surface scanning, affects the image contrast.

Fig. 7 shows sequentially recorded images of the sample $(7 \times 7)_N$ surface (exposure 5L) when scanning the same area at different voltages between the sample and the probe, while the working tunneling current was kept constant at a level of 0.025nA.

Fig. 7a-c clearly show that the color contrast between the corner and central adatoms decreases with voltage increasing. Note that the images shown here are presented with a fixed range of z-coordinate variation. It is clear that the dynamics of the height profiles with such variation of voltage (Fig. 7d) is consistent with a decrease in the image contrast. In the presented profiles, it is important to pay attention to the fact that with increasing voltage (curve + 2.1 V), the difference in heights in the corresponding maxima for the central adatom and corner adatom disappeared (in some areas the difference even changed to the opposite). In addition, at voltages of + 1.5 V and + 2.1 V, a peak was clearly manifested itself at the place of the dip in the profile at a voltage of + 1 V, that is, it became possible to resolve an atom that was not observed at + 1 V. It should also be emphasized that such a change in color contrast (and profiles) is not associated with any degradation of the surface when sequentially scanning the same area, since a return, for example, to a low voltage leads to the reproduction of a previously observed contrast, moreover, the contrast is reproduced when reusing one or another voltage. In our opinion, the discovered effect indicates that the dark stripes in the area of the central adatoms of the $(7 \times 7)_N$ structure, which look like “morphological pits”, in fact correspond to atoms located approximately at the same height with corner adatoms.

A similar effect of changing the color contrast with varying voltage between the probe and the sample is clearly observed at the boundary

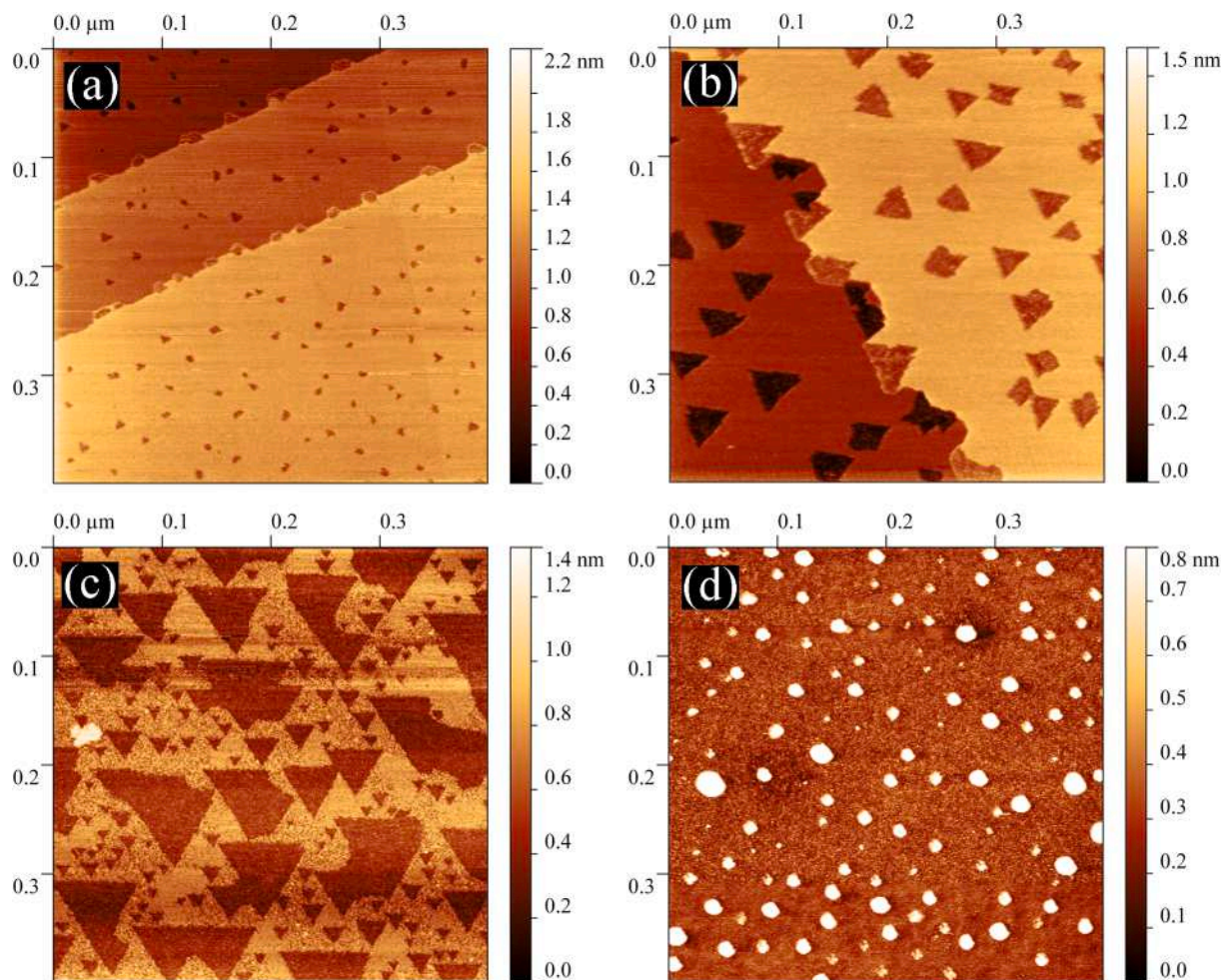


Fig. 5. STM images of a surface with (8×8) structures nuclei at various exposures in ammonia: (a) 5 L; (b) 15 L; (c) 21 L, (d) greater than 40 L. For the increased exposures (greater than 30 L) the formation of 3D clusters of amorphous silicon nitride is visible, it looks like white islands (d). Voltage is + 2 V, tunneling current is 0.025 nA.

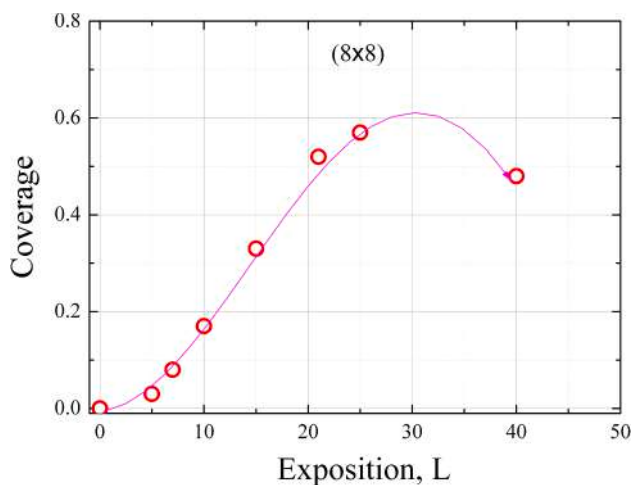


Fig. 6. Evolution of the surface coverage by the (8×8) structure with increasing of ammonia exposure. The decrease of the (8×8) coating is associated with the amorphous Si_3N_4 formation.

between the regions $(7 \times 7)_N$ and (8×8) structures. Fig. 8 demonstrates the measurements data on a sample obtained as a result of ammonia exposure of the surface with a dose of 7L. Here, as in the previous case,

the images obtained by sequential scanning of the same area of the sample at different positive bias voltages on the sample are presented.

These images clearly show a significant decrease in contrast between light $(7 \times 7)_N$ and dark (8×8) areas with increasing bias voltage. It is convenient to consider this effect by comparing the height profiles measured at this boundary. The profiles of the normalized height (by the coefficient given in the experimental part) along the lines marked in the images in Fig. 8 are shown in Fig. 8(e).

It is seen that the magnitude of the measured step significantly depends on the voltage across the tunnel gap. The apparent “deep morphological pit” with a depth of 4.9 \AA , observed at + 1 V, becomes the “shallow” only 1.7 \AA when the voltage rises to + 2.5 V. A similar effect is equally manifested on different samples after treatment in ammonia at different exposures, if it is possible to find coexisting $(7 \times 7)_N$ and (8×8) structures on such surfaces. Note also that the color contrast and/or step size returns to the previous value when a certain voltage is restored after voltage variation in one direction or another.

Thus, the seeming “morphological step” [44,45] is not actually a step. Such phenomena can be associated with a change in the local density of states of the surface during the formation of nitride $(7 \times 7)_N$ and (8×8) structures; therefore, it is necessary to study the behavior of the density of electronic states of the surfaces.

The behavior of the tunneling current is quantitatively described in the one-dimensional WKB (Wentzel – Kramers – Brillouin) approximation by the following expressions [60]:

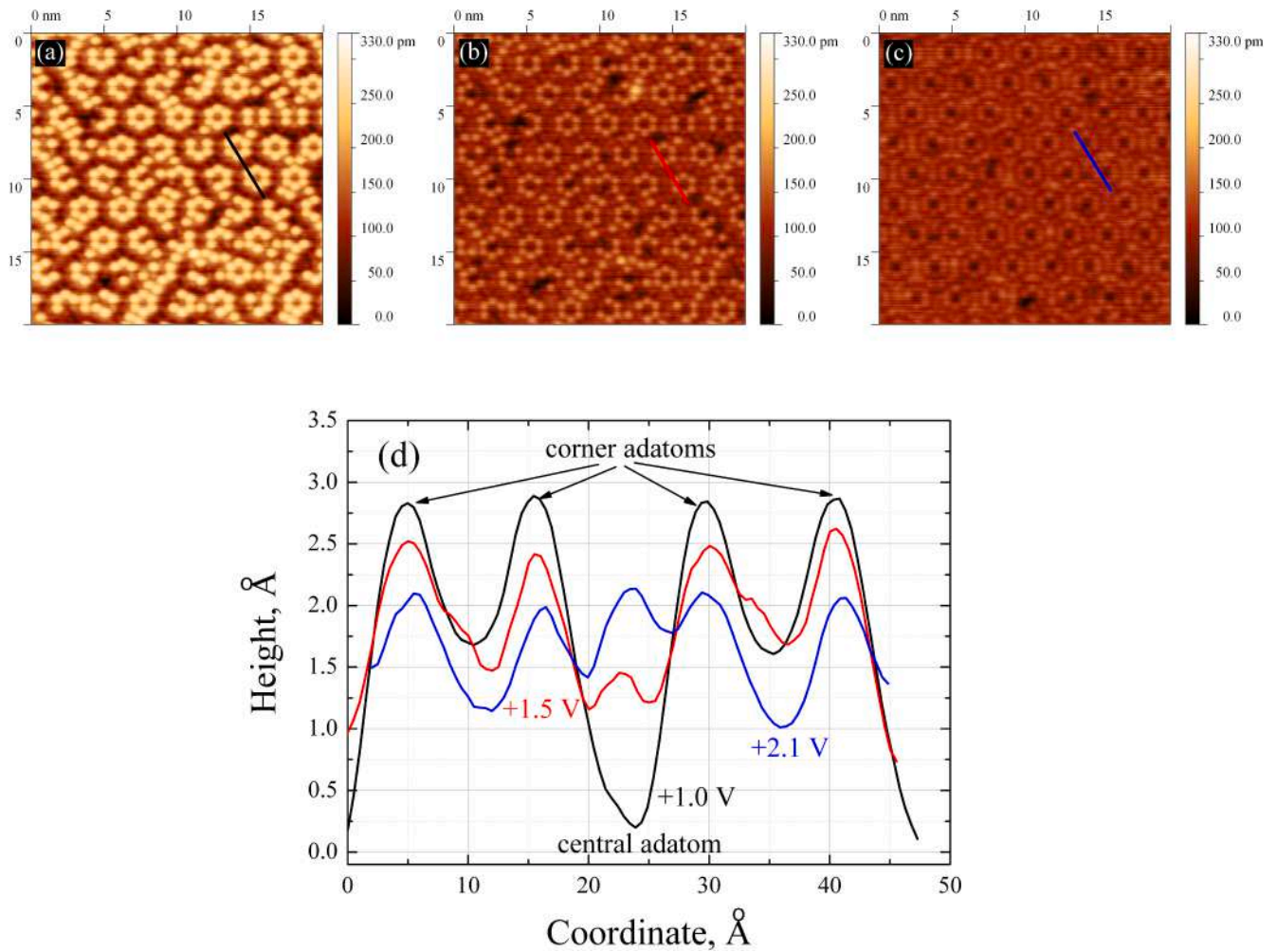


Fig. 7. STM images of a surface area $(7 \times 7)_N$ structure obtained at different operating voltages (biases) (a) + 1.0 V, (b) + 1.5 V, (c) + 2.1 V; (d) height profiles of the $(7 \times 7)_N$ structure at different voltages. The lines along which the profiles were measured are shown in images (a) - (c).

$$I(V, z) \sim \int_0^V \rho_s(E) \cdot \rho_t(E - V) \cdot T(E, V, z) dE \quad (1)$$

and

$$T(E, V, z) = \exp \left[-\sqrt{\alpha \cdot \left(\varphi + \frac{V}{2} - E \right)} \cdot z \right] \quad (2)$$

where φ is the height of the tunneling barrier at zero bias and $\alpha = 8 \text{ m/h}^2$, z is the distance from the probe to the surface, or the tunneling gap, E is the integration variable that covers the energy range corresponding to the difference between the Fermi levels of the probe and the sample. The function $T(E, V, z)$ describes the transmission coefficient of the tunneling barrier (it is assumed that the barrier is trapezoidal) at a distance z from the probe to the sample surface, $\rho_s(E)$ is the density of states of the sample. The density of states of the probe $\rho_t(E-V)$ is considered to be a smooth, low-varying function. The equations also imply the dependence of the current on the lateral coordinates (x, y) , but for brevity they are not explicitly written in the formula.

The above formula shows how exactly the contributions to the tunneling current of the spectrum of the surface density of states and the tunneling distance are “entangled”, and this allows a better idea to explain the role of current feedback in the formation of image contrast during scanning in an STM. By knowing the tunneling gap and the difference $\rho_s(E)$ in the spectra at different points of the surface, it is possible to calculate the tunneling currents at these points for a fixed tunneling gap between the probe and the surface, or the corresponding

displacements of the probe at a fixed tunneling current, i.e. in the presence of current feedback.

3.3. Explanation of the observed contrast of STM images based on local spectra

Let’s consider couple specific examples of contrast formation. When measuring the $(7 \times 7)_N$ structure, we take into account that the adatoms on the initial clean (7×7) silicon surface are at the same height. We also assume that morphological changes on the $(7 \times 7)_N$ structure are insignificant, since comparing Fig. 8a and Fig. 8c, we see a change in the color contrast between the central and corner adatoms with increasing voltage, which cannot be associated with real morphological features. Let us compare the STS spectra measured on small surface areas corresponding to the lateral positions of the central and corner adatoms. In Fig. 9 are shown fragments of the spectra of the local density of states at positive biases on the samples for the STM images presented above (see [supplementary materials Part 7](#)).

Here we are using the well-known statement that the normalized differential resistance $(dI/dV)/(I/V)$ is proportional to the local density of states [61]. Fig. 9a shows that in the spectrum of the density of states in the range from 0 to + 1 V, the total area under the red curve is larger than under the black one. It means that a larger tunneling current is expected for corner adatoms, and, therefore, will cause a corresponding compensating displacement of the probe from the surface, which will appear in image as a lighter place (or “high place”) in relation to the

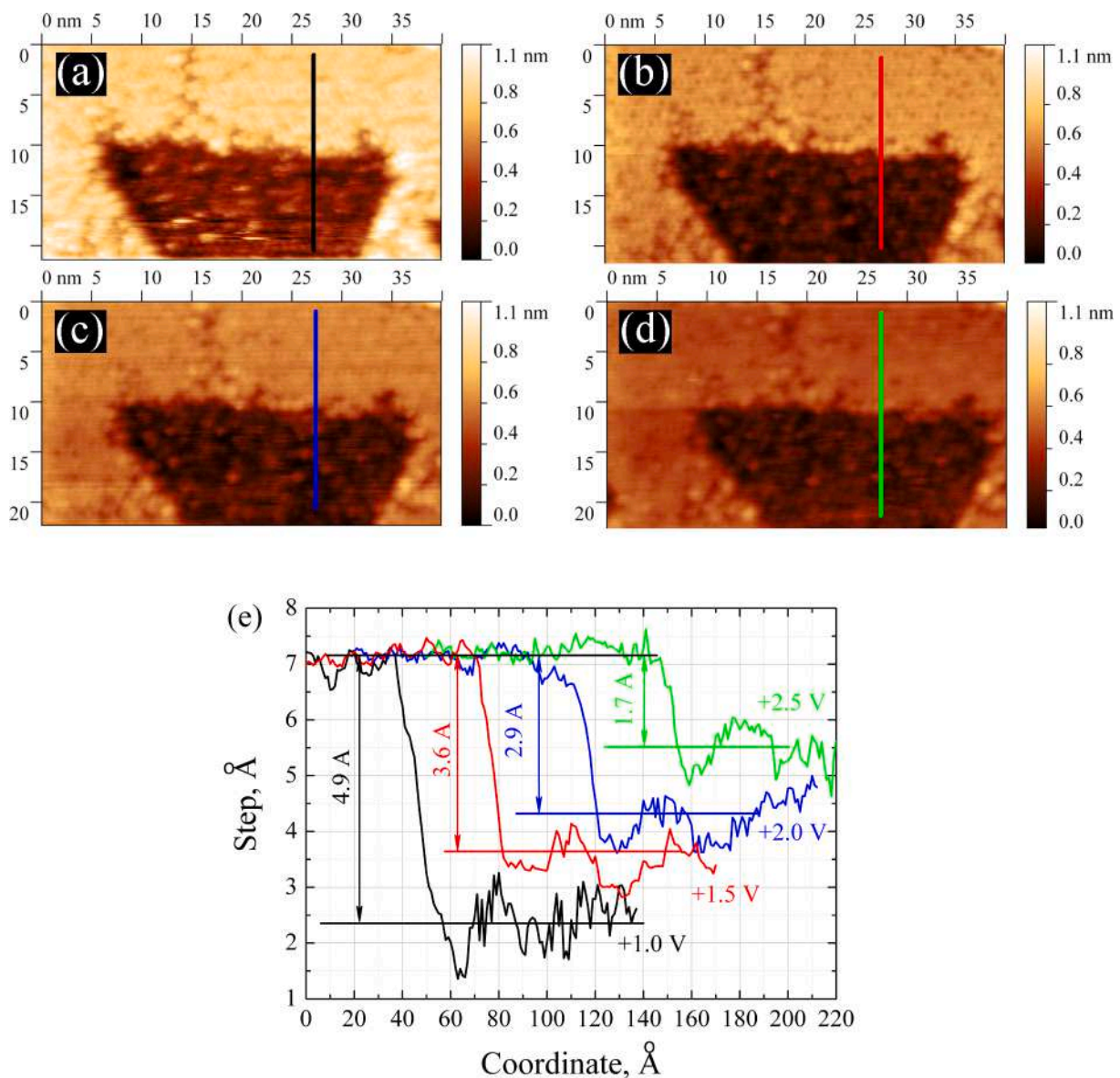


Fig. 8. Change in color contrast on STM images of the $(7 \times 7)_N/(8 \times 8)$ boundary with a change in bias voltage: (a) +1.0 V, (b) +1.5 V, (c) +2.0 V, (d) +2.5 V; (e) Profiles of normalized “height” at the boundary of $(7 \times 7)_N$ and (8×8) structures at different voltages across the tunnel gap. The curves are deliberately shifted along the abscissa for better viewability.

darker central adatom place. In turn, in the range from 0 to +2.1 V, the area under the red curve is close to the area under the black curve (since the shaded area in black roughly compensates for the shaded area in red). Then a small difference in tunneling currents at the both places on the surface is expected, and the color contrast between the corresponding places vanishes at this scanning voltage.

Similar reasoning is applicable for the case when the contrast appears at the boundary between the $(7 \times 7)_N$ and (8×8) structures (see Figs. 8 and 9). The corresponding spectra are shown in Fig. 9(b). It can be seen that at low voltages, the area under the red curve (for example, from 0 to +1 V) is significantly larger than under the black one. This difference decreases with increasing voltage, and above a certain voltage (+2.0 V) the black curve lies even above the red one. There is an alignment of tunneling currents and a corresponding disappearing of the contrast in STM images.

Thus, the observed contrast in STM images can be fully explained on the basis of accounting only the local density of electronic states. Of course, the contrast can be due to a morphological contribution, for example, when measuring the contrast of the steps on a clean silicon

surface as described above.

3.4. Evolution of the local electronic states of a silicon surface upon exposure under ammonia flux

Variation of the composition and structure of the surface should necessarily lead to changes in the electronic states of the surface. Varying the exposure of the surface in ammonia a change in the local spectra of the density of electronic states was observed (Fig. 10).

The blue and green spectra in Fig. 10 were obtained from surfaces with the $(7 \times 7)_N$ structure treated by ammonia at exposures 3L and 7L, respectively. The peaks shifted from the initial position of the S1 and S2 peaks corresponded to the clean silicon surface toward the position of the characteristic peak (-1.1 eV at red curve) belonged to the structure (8×8) . The shift is stronger for a higher dose, although STM images of the $(7 \times 7)_N$ structures looked like very similar. In Fig. 10 is also shown that as nitride (8×8) structure is formed a bandgap appears (about 2 eV) between the characteristic peak -1.1 eV and the peak in the zone of free states +1.4 eV. For the $(7 \times 7)_N$ structure the energy position of the

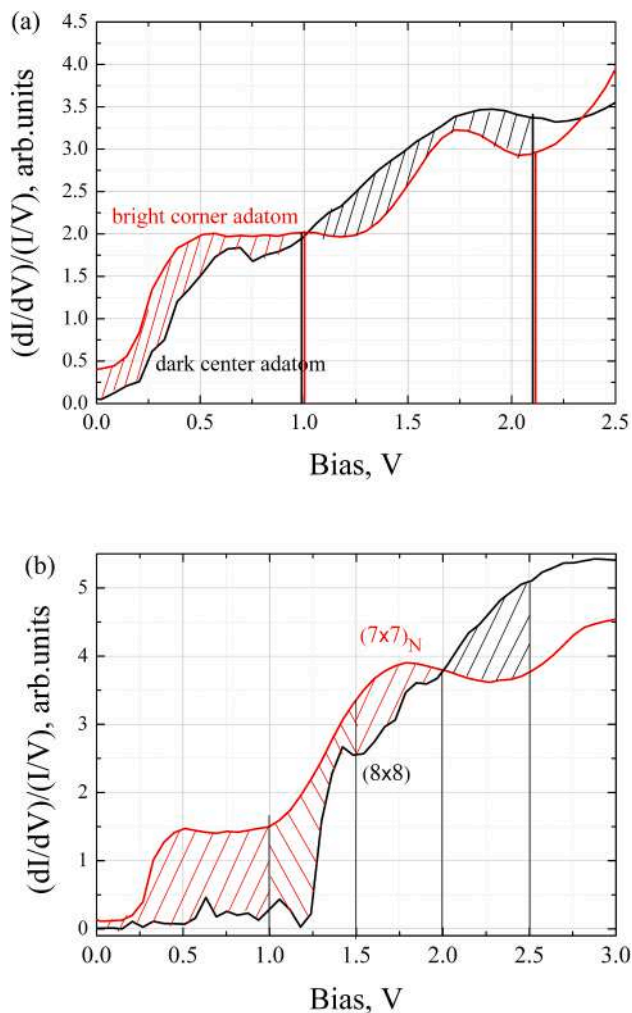


Fig. 9. Comparison of the STS spectra and areas under the curves (i.e., estimation of the expected tunneling current) at different biases in the tunneling gap for: (a) dark central (black curve) and light corner adatoms of the $(7 \times 7)_N$ structure, (b) black curve for the (8×8) structure and red curve for the $(7 \times 7)_N$ structure. The differences in areas are shaded.

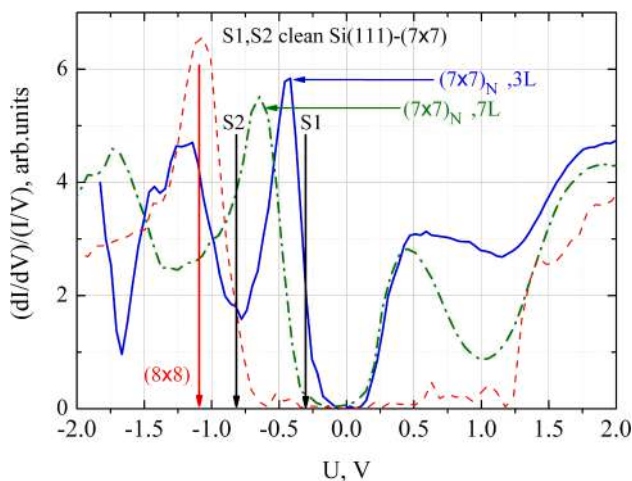


Fig. 10. Density of states spectra for $(7 \times 7)_N$ and (8×8) structures obtained at different surface exposure under ammonia flow at 1000°C . The positions of the known peaks (S1, S2) in the density of states of (7×7) structure are indicated by black arrows.

peaks (blue spectrum -0.4 eV, -1.2 eV and green spectrum -0.7 eV, -1.7 eV) are located between the peaks of pure silicon and (8×8) phase. After the formation of the (8×8) phase these peaks “disappear”. Therefore, it can be assumed that these local electronic states belong to some building fragments (like $\text{Si}_x\text{N}_y\text{H}_z$ chains or $\text{Si}_3\text{N}_3\text{H}_3$ aromatic rings) from which the phase (8×8) is formed while the dose increased. An ensemble of such fragments on the surface is usually called as a lattice gas. Lateral interaction in the lattice gas provides a phase transition to a condensed ordered phase (8×8) [62]. These local electronic states as well as the characteristic states of the (8×8) phase, positioning comparatively high in energy (i.e. close to the Fermi level), are the dangling bonds of silicon or π -bonds of Si-Si and Si-N. The σ -bonds of Si-Si and Si-N are significantly deeper in energy.

3.5. Atoms reactivity on the (1×1) and (7×7) structures

During nitridation process of a silicon surface with (7×7) structure, it was usually believed that central adatoms are more chemically reactive with ammonia than corner adatoms [39–41]. In our experiments, nitridation process was carried out at a high temperature with the (1×1) structure, on which all adatoms are equivalent, and the mobile Si adatoms are the highest reactivity atoms [27]. Hence a homogeneous disordered high-temperature silicon nitride phase of low concentration and strongly enriched by silicon is formed at these high temperature conditions. Nevertheless, STM images of $(7 \times 7)_N$ structure are very similar to images obtained at low (room) temperature nitridation. Let us emphasized one more time that for the (1×1) structure at high temperature there are no any differences, including reactivity, between the central and corner adatoms because the adatoms of these kinds are definitely absent. The structure $(7 \times 7)_N$ is formed upon cooling the sample surface as a result of the phase transition from (1×1) to (7×7) structure at temperatures below 830°C . It is known that the corner holes are the most stable fragment of the DAS structure [63,64]. So, in our case as initial stage of the $(7 \times 7)_N$ structure formation the non reacted silicon atoms forms the corner holes surrounded by silicon adatoms, this process corresponds to the brighter areas formation in the STM images. On the other hand the central area between the corner holes is filled by mixture of silicon atoms and of appeared $\text{Si}_x\text{N}_y\text{H}_z$ fragments (for the future (8×8) structure) with various compositions - chains, rings, and other configurations, and this process corresponds to the formation of darker central areas. This is the possible reason of the similarity of the STM images obtained by high and low temperatures nitridation. In the appearing silicon nitride fragments, silicon atoms are in sp^2 hybridization state, nitrogen atoms are mainly in sp hybridization state. At a certain critical concentration of such fragments the formation of the (8×8) structure become possible as a result of the phase transition.

4. Conclusion

In summary, the Si (111) surface nitridation process at high temperatures depending on the ammonia dose was studied by the STM/STS techniques. The intermediate phases $(7 \times 7)_N$ arising at doses $< 5\text{L}$ preceding the (8×8) structure formation are determined. The $(7 \times 7)_N$ phase appears in the STM images as result of phase transition (1×1) to $(7 \times 7)_N$ upon cooling from a high nitridation temperature to room temperature. It is discovered that the increase of the (8×8) structure coverage is terminated at the dose of 30 L. The termination is explained by the depletion of the equilibrium concentration of mobile silicon adatoms. It is shown within framework of the WKB tunneling current theory that the (8×8) structure is formed over the silicon surface but not in the etching pits on the surface. The peak shifts of local electronic states as a function of the ammonia dose is found. The nature of the peaks is proposed to associate with the electronic states of dangling bonds and/or π -bonds that incorporated into $\text{Si}_x\text{N}_y\text{H}_z$ fragments. In turn, these fragments are the building blocks for the upcoming (8×8) structure.

CRediT authorship contribution statement

Vladimir Mansurov: Methodology, Investigation, Formal analysis, Writing – original draft. **Yury Galitsyn:** Conceptualization, Methodology, Writing – review & editing. **Timur Malin:** Resources, Visualization. **Sergey Teys:** Investigation, Resources. **Denis Milakhin:** Formal analysis, Visualization. **Konstantin Zhuravlev:** Supervision, Funding acquisition, Writing – review & editing.

Declaration of Competing Interest

The authors declare that they have no known competing financial interests or personal relationships that could have appeared to influence the work reported in this paper.

Acknowledgments

The research was funded by RFBR and Novosibirsk region, project number 20-42-540011.

Appendix A. Supplementary material

Supplementary data to this article can be found online at <https://doi.org/10.1016/j.apsusc.2021.151276>.

References

- [1] A.K. Geim, Graphene: status and prospects, *Science* 324 (5934) (2009) 1530–1534, <https://doi.org/10.1126/science.1158877>.
- [2] F. Schwierz, Graphene transistors, *Nat. Nanotechnol.* 5 (7) (2010) 487–496, <https://doi.org/10.1038/nnano.2010.89>.
- [3] W. Zhu, D. Neumayer, V. Perebinos, P. Avouris, Silicon Nitride Gate Dielectrics and Band Gap Engineering in Graphene Layers, *Nano Lett.* 10 (9) (2010) 3572–3576, <https://doi.org/10.1021/nl101832y>.
- [4] J. Zhou, Q. Wang, Q. Sun, X.S. Chen, Y. Kawazoe, P. Jena, Ferromagnetism in Semihydrogenated Graphene Sheet, *Nano Lett.* 9 (11) (2009) 3867–3870, <https://doi.org/10.1021/nl9020733>.
- [5] A. Du, S. Sanvito, S.C. Smith, First-Principles Prediction of Metal-Free Magnetism and Intrinsic Half-Metallicity in Graphitic Carbon Nitride, *Phys. Rev. Lett.* 108 (2012), 197207, <https://doi.org/10.1103/PhysRevLett.108.197207>.
- [6] M.H.V. Huynh, M.A. Hiskey, J.G. Archuleta, E.L. Roemer, Preparation of Nitrogen Rich Nanolayered, Nanoclustered, and Nanodendritic Carbon Nitrides, *Angew. Chem.* 117 (5) (2005) 747–749, [https://doi.org/10.1002/\(ISSN\)1521-375710.1002/ange.v117:510.1002/ange.200461758](https://doi.org/10.1002/(ISSN)1521-375710.1002/ange.v117:510.1002/ange.200461758).
- [7] X. Li, S. Zhang, Q. Wang, Stability and physical properties of a tri-ring based porous g-C₃N₃ sheet, *Phys. Chem. Chem. Phys.* 15 (2013) 7142–7146, <https://doi.org/10.1039/C3CP44660C>.
- [8] P. Niu, G. Liu, H.-M. Cheng, Nitrogen Vacancy-Promoted Photocatalytic Activity of Graphitic Carbon Nitride, *J. Phys. Chem. C* 116 (20) (2012) 11013–11018, <https://doi.org/10.1021/jp301026y>.
- [9] P. Niu, L. Zhang, G. Liu, H.-M. Cheng, Graphene-like Carbon Nitride Nanosheets for Improved Photocatalytic Activities, *Adv. Funct. Mater.* 22 (22) (2012) 4763–4770, <https://doi.org/10.1002/adfm.v22.2210.1002/adfm.201200922>.
- [10] X. Wang, S. Blechert, M. Antonietti, Polymeric Graphitic Carbon Nitride for Heterogeneous Photocatalysis, *ACS Catal.* 2 (8) (2012) 1596–1606, <https://doi.org/10.1021/cs300240x>.
- [11] X. Li, J. Zhou, Q. Wang, Y. Kawazoe, P. Jena, Patterning Graphitic C–N Sheets into a Kagome Lattice for Magnetic Materials, *J. Phys. Chem. Lett.* 4 (2) (2013) 259–263, <https://doi.org/10.1021/jz3018804>.
- [12] D.M. Teter, R.J. Hemley, Low-Compressibility Carbon Nitrides, *Science* 271 (5245) (1996) 53–55, <https://doi.org/10.1126/science.271.5245.53>.
- [13] T. Botari, W.P. Huhn, V.-H. Lau, B.V. Lotsch, V. Blum, Thermodynamic Equilibria in Carbon Nitride Photocatalyst Materials and Conditions for the Existence of Graphitic Carbon Nitride g-C₃N₄, *Chem. Mater.* 29 (10) (2017) 4445–4453, <https://doi.org/10.1021/acs.chemmater.7b0096510.1021/acs.chemmater.7b00965.s001>.
- [14] G. Algara-Siller, N. Severin, S.Y. Chong, T. Björkman, R.G. Palgrave, A. Laybourn, M. Antonietti, Y.Z. Khimyak, A.V. Krashenninnikov, J.P. Rabe, U. Kaiser, A. I. Cooper, A. Thomas, M.J. Bojdy, Triazine-Based Graphitic Carbon Nitride: a Two-Dimensional Semiconductor, *Angew. Chem. Int. Ed.* 53 (29) (2014) 7450–7455, <https://doi.org/10.1002/ange.201402191>.
- [15] K. Abersfelder, A.J.P. White, H.S. Rzepa, D.A. Scheschkewitz, Tricyclic Aromatic Isomer of Hexasilabenzene, *Science* 327 (2010) 564–566, <https://doi.org/10.1126/science.1181771>.
- [16] A. Kuhn, P. Sreeraj, R. Pottgen, H.D. Wiemhofer, M. Wilkening, P. Heitjans, Li NMR Spectroscopy on Crystalline Li₂Si₇: Experimental Evidence for the Aromaticity of the Planar Cyclopentadienyl-Analogous Si₆⁶⁻ Rings, *Angew. Chem. Int. Ed.* 50 (2011) 12099–12102, <https://doi.org/10.1002/anie.201105081>.
- [17] M. Moteki, S. Maeda, K. Ohno, Systematic Search for Isomerization Pathways of Hexasilabenzene for Finding Its Kinetic Stability, *Organomet.* 28 (7) (2009) 2218–2224, <https://doi.org/10.1021/om800881y>.
- [18] M. Nabati, M. Mahkam, DFT Study of the Six-Membered Heterocyclic Si₆N_{6-m}H_n (n = 0–6): Stability and Aromaticity, *Org. Chem. Res.* 2 (2016) 70–80, <https://doi.org/10.22036/org.chem.2016.13580>.
- [19] Y. Guo, S.H. Zhang, Q. Wang, Electronic and Optical Properties of Silicon Based Porous Sheets, *Phys. Chem. Chem. Phys.* 16 (2014) 16832–16836, <https://doi.org/10.1039/C4CP01491J>.
- [20] V.G. Mansurov, Y.G. Galitsyn, T.V. Malin, S.A. Teys, E.V. Fedosenko, A. S. Kozhukhov, K.S. Zhuravlev, I. Cora, B. Pécz, Ildikó Cora, Béla Pécz, Formation of a Graphene-Like SiN Layer on the Surface Si(111), *Semiconductors* 52 (12) (2018) 1511–1517, <https://doi.org/10.1134/S1063782618120151>.
- [21] V. G. Mansurov, Yu. G. Galitsyn, T. V. Malin, S. A. Teys, K. S. Zhuravlev, Ildikó Cora, Béla Pécz, Van der Waals and Graphene-Like Layers of Silicon Nitride and Aluminum Nitride, in *2D Materials*, C. Wongchoosuk (Editor), IntechOpen, London, 2019. DOI: 10.5772/intechopen.81775.
- [22] M. Nishijima, H. Kobayashi, K. Edamoto, M. Onchi, Reactions of NO with the Si(111) (7×7) surface: EELS, LEED and AES studies, *Surf. Sci.* 137 (2–3) (1984) 473–490, [https://doi.org/10.1016/0039-6028\(84\)90524-7](https://doi.org/10.1016/0039-6028(84)90524-7).
- [23] M. Nishijima, K. Edamoto, Y. Kubota, H. Kobayashi, M. Onchi, Adsorbates on the Si(111) (7×7) surface - EELS/LEED/AES studies, *Surf. Sci.* 158 (1–3) (1985) 422–437, [https://doi.org/10.1016/0039-6028\(85\)90320-6](https://doi.org/10.1016/0039-6028(85)90320-6).
- [24] K. Edamoto, S. Tanaka, M. Onchi, M. Nishijima, Electron energy-loss spectra of Si(111) reacted with nitrogen atoms, *Surf. Sci.* 167 (2–3) (1986) 285–296, [https://doi.org/10.1016/0039-6028\(86\)90705-3](https://doi.org/10.1016/0039-6028(86)90705-3).
- [25] Y. Morita, H. Tokumoto, Origin of the 8/3×8/3 superstructure in STM images of the Si(111)-8×8: N surface, *Surf. Sci.* 443 (1999) L1037–L1042, [https://doi.org/10.1016/S0039-6028\(99\)01021-3](https://doi.org/10.1016/S0039-6028(99)01021-3).
- [26] V.G. Mansurov, T.V. Malin, Y.G. Galitsyn, K.S. Zhuravlev, Graphene-like AlN layer formation on (111)Si surface by ammonia molecular beam epitaxy, *J. Cryst. Growth.* 428 (2015) 93–97, <https://doi.org/10.1016/j.jcrysgro.2015.07.030>.
- [27] V.G. Mansurov, T.V. Malin, Y.G. Galitsyn, A.A. Shklyayev, K.S. Zhuravlev, Kinetics and thermodynamics of Si(111) surface nitridation in ammonia, *J. Cryst. Growth.* 441 (2016) 12–17, <https://doi.org/10.1016/j.jcrysgro.2016.02.007>.
- [28] I. Cora, A. Kovács, V.G. Mansurov, T.V. Malin, Y.G. Galitsyn, K.S. Zhuravlev, B. Pécz, Microscopy of thin AlN layers grown by MBE on (111) silicon, *European Crystallography Congress: Proceedings 1* (2016) 626–627, <https://doi.org/10.1002/9783527808465.EMC2016.6215>.
- [29] S.P. Murarka, C.C. Chang, A.C. Adams, Thermal Nitridation of Silicon in Ammonia Gas: Composition and Oxidation Resistance of the Resulting Films, *J. Electrochem. Soc.* 126 (6) (1979) 996–1003, <https://doi.org/10.1149/1.2129223>.
- [30] C.-Y. Wu, C.-W. King, M.-K. Lee, C.-T. Chen, Growth Kinetics of Silicon Thermal Nitridation, *J. Electrochem. Soc.* 129 (7) (1982) 1559–1563, <https://doi.org/10.1149/1.2124207>.
- [31] C. Maillot, H. Roulet, G. Dufour, Thermal nitridation of silicon: An XPS and LEED investigation, *J. Vac. Sci. Technol. B* 2 (1984) 316–319, <https://doi.org/10.1116/1.582816>.
- [32] A. Wierzbicka, G. Tchutchulashvili, M. Sobanska, K. Klosek, R. Minikayev, J. Z. Domagala, J. Borysiuk, Z.R. Zytkevicz, Arrangement of GaN nanowires on Si(001) substrates studied by X-ray diffraction: Importance of silicon nitride interlayer, *Appl. Surf. Sci.* 425 (2017) 1014–1019, <https://doi.org/10.1016/j.apsusc.2017.07.075>.
- [33] A.J. Van Bommel, F. Meyer, A low energy electron diffraction study of the PH₃ adsorption on the Si(111) surface, *Surf. Sci.* 8 (4) (1967) 381–398, [https://doi.org/10.1016/0039-6028\(67\)90046-5](https://doi.org/10.1016/0039-6028(67)90046-5).
- [34] B. Rottger, R. Kliese, H. Neddermeyer, Adsorption and reaction of NO on Si(111) studied by scanning tunneling microscopy, *J. Vac. Sci. Technol. B* 14 (1996) 1051–1054, <https://doi.org/10.1116/1.588398>.
- [35] H. Ahn, C.L. Wu, S. Gwo, C.M. Wei, Y.C. Chou, Structure Determination of the Si₃N₄/Si(111)-(8×8) Surface: A Combined Study of Kikuchi Electron Holography, Scanning Tunneling Microscopy, and *ab initio* Calculations, *Phys. Rev. Lett.* 86 (2001) 2818–2821, <https://doi.org/10.1103/PhysRevLett.86.2818>.
- [36] X.S. Wang, G. Zhai, J. Yang, N. Cue, Crystalline Si₃N₄ thin films on Si(111) and the 4×4 reconstruction on Si₃N₄(0001), *Phys. Rev. B* 60 (1999) R2146–R2149, <https://doi.org/10.1103/PhysRevB.60.R2146>.
- [37] X.-S. Wang, G. Zhai, J. Yang, L. Wang, Y. Hu, Z. Li, J.C. Tang, X. Wang, K.K. Fung, N. Cue, Nitridation of Si(111), *Surf. Sci.* 494 (2) (2001) 83–94, [https://doi.org/10.1016/S0039-6028\(01\)01409-1](https://doi.org/10.1016/S0039-6028(01)01409-1).
- [38] S. Shetty, S.M. Shivaprasad, Early stages of plasma induced nitridation of Si(111) surface and study of interfacial band alignment, *J. Appl. Phys.* 119 (2016), 055306, <https://doi.org/10.1063/1.4941102>.
- [39] R. Wolkow, P.h. Avouris, Atom-Resolved Surface Chemistry Using Scanning Tunneling Microscopy, *Phys. Rev. Lett.* 60 (1988) 1049, <https://doi.org/10.1103/PhysRevLett.60.1049>.
- [40] P.h. Avouris, R. Wolkow, Atom-resolved surface chemistry studied by scanning tunneling microscopy and spectroscopy *Phys. Rev. B* 39 (1989) 5091, <https://doi.org/10.1103/PhysRevB.39.5091>.
- [41] P. Avouris, Atom-Resolved Surface Chemistry Using the Scanning Tunneling Microscope, *J. Phys. Chem.* 94 (6) (1990) 2246–2256, <https://doi.org/10.1021/j100369a011>.
- [42] C.-L. Wu, J.-L. Hsieh, H.-D. Hsueh, S. Gwo, Thermal nitridation of the Si(111)-(7×7) surface studied by scanning tunneling microscopy and spectroscopy, *Phys. Rev. B* 65 (2002), 045309, <https://doi.org/10.1103/PhysRevB.65.045309>.

- [43] C.-L. Wu, W.-S. Chen, Y.-H. Su, N_2 -plasma nitridation on Si(111): Its effect on crystalline silicon nitride growth, *Surf. Sci.* 606 (2012) L51–L54, <https://doi.org/10.1016/j.susc.2012.03.004>.
- [44] S. Gangopadhyay, T. Schmidt, J. Falta, Initial stage of silicon nitride nucleation on Si(111) by rf plasma-assisted growth, e-J, *Surf. Sci. Nanotech.* 4 (2006) 84–89, <https://doi.org/10.1380/ejssnt.2006.84>.
- [45] S. Gangapayhyay, Crystalline Silicon Nitride Films on Si(111): Growth Mechanism, Surface Structure and Chemistry down to Atomic Scale, in *Multilayer Thin Films - Versatile Applications for Materials Engineering*, Sukumar Basu (Editor), IntechOpen, London, 2020. DOI: 10.5772/intechopen.89412.
- [46] T.L. Petrenko, V.P. Bryksa, I.V. Dyka, V.P. Kladko, A.E. Belyaev, A.V. Kuchuk, Microscopic mechanisms of Si(111) surface nitridation and energetics of $Si_3N_4/Si(111)$ interface, *Appl. Surf. Sci.* 483 (2019) 302–312, <https://doi.org/10.1016/j.apsusc.2019.03.239>.
- [47] M.-H. Kang, Theory of the site-selective reaction of NH_3 with Si(111)-(7 \times 7), *Phys. Rev. B* 68 (2003), 205307, <https://doi.org/10.1103/PhysRevB.68.205307>.
- [48] Rong-Li Lo, Chun-Ming Chang, Mon-Shu Ho, NH_2 and NH bonding sites determined by STM-induced activation on the NH_3 -reacted Si(111)-7 \times 7 surface, *Phys. Rev. B* 76 (2007), 113305, <https://doi.org/10.1103/PhysRevB.76.113305>.
- [49] X. Wang, X. Xu, Mechanisms for NH_3 Decomposition on the Si(111)-7 \times 7 Surface: A DFT Cluster Model Study, *J. Phys. Chem. C* 111 (2007) 16974–16981, <https://doi.org/10.1021/jp075193s>.
- [50] Ph. Sautet, Images of Adsorbates with the Scanning Tunneling Microscope: Theoretical Approaches to the Contrast Mechanism, *Chem. Rev.* 97 (1997) 1097–1116, <https://doi.org/10.1021/cr9600823>.
- [51] Philippe Sautet, Atomic adsorbate identification with the STM: a theoretical approach, *Surf. Sci.* 374 (1-3) (1997) 406–417, [https://doi.org/10.1016/S0039-6028\(96\)01239-3](https://doi.org/10.1016/S0039-6028(96)01239-3).
- [52] R. Flammini, P. Allegrini, F. Wiame, R. Belkhou, F. Ronci, S. Colonna, D. M. Trucchi, F. Filippone, S.K. Mahatha, P.M. Sheverdyeva, P. Moras, Nearly-free electronlike surface resonance of a β - $Si_3N_4(0001)/Si(111)$ -8 \times 8 interface, *Phys. Rev. B* 91 (2015), 075303, <https://doi.org/10.1103/PhysRevB.91.075303>.
- [53] J.W. Kim, H.W. Yeom, Surface and interface structures of epitaxial silicon nitride on Si(111), *Phys. Rev. B* 67 (2003), 035304, <https://doi.org/10.1103/PhysRevB.67.035304>.
- [54] Daisuke Matsushita, Hiroya Ikeda, Akira Sakai, Shigeaki Zaima, Yukio Yasuda, Scanning tunneling microscopy/scanning tunneling spectroscopy of initial nitridation process of Si(100)-2 \times 1 surfaces, *Thin Solid Films* 369 (1-2) (2000) 293–296, [https://doi.org/10.1016/S0040-6090\(00\)00882-8](https://doi.org/10.1016/S0040-6090(00)00882-8).
- [55] Daisuke Matsushita, Hiroya Ikeda, Akira Sakai, Shigeaki Zaima, Yukio Yasuda, Atomic-Scale Characterization of Nitridation Processes on Si(100)-2 \times 1 Surfaces by Radical Nitrogen, *Jpn. J. Appl. Phys.* 40 (Part 1, No. 4B) (2001) 2827–2829, <https://doi.org/10.1143/JJAP.40.2827>.
- [56] Hiroya Ikeda, Daisuke Matsushita, Shinya Naito, Kenji Ohmori, Akira Sakai, Shigeaki Zaima, Yukio Yasuda, Growth Processes and Electrical Characteristics of Silicon Nitride Films Formed on Si(100) by Radical Nitrogen, *Jpn. J. Appl. Phys.* 41 (Part 1, No. 4B) (2002) 2463–2467, <https://doi.org/10.1143/JJAP.41.2463>.
- [57] H. Kondo, K. Kawai, A. Sakai, M. Hori, S. Zaima, Y. Yasuda, Growth and energy bandgap formation of silicon nitride films in radical nitridation, *Jpn. J. Appl. Phys.* 46 (1R) (2007) 71–75, <https://doi.org/10.1143/JJAP.46.71>.
- [58] R.J. Hamers, R.M. Tromp, J.E. Demuth, Surface Electronic Structure of Si(111)-(7 \times 7) Resolved in Real Space, *Phys. Rev. Lett* 56 (1986) 1972, https://doi.org/10.1007/978-94-011-1812-5_12.
- [59] H. Guo, Y. Wang, S. Du, H. Gao, High-resolution scanning tunneling microscopy imaging of Si(111)-7 \times 7 structure and intrinsic molecular states, *J. Phys.: Condens. Matter* 26 (2014), 394001, <https://doi.org/10.1088/0953-8984/26/39/394001>.
- [60] B. Koslowski, C. Dietrich, A. Tschetschetkin, P. Ziemann, Evaluation of scanning tunneling spectroscopy data: Approaching a quantitative determination of the electronic density of states, *Phys. Rev. B* 75 (2007), 035421, <https://doi.org/10.1103/PhysRevB.75.035421>.
- [61] R.M. Feenstra, J.A. Stroscio, A.P. Fein, Tunneling spectroscopy of the Si(111)-2 \times 1 surface, *Surf. Sci.* 181 (1987) 295, [https://doi.org/10.1016/0039-6028\(87\)90170-1](https://doi.org/10.1016/0039-6028(87)90170-1).
- [62] A. Zangwill, *Physics at Surfaces*, Cambridge University Press, Chapter 11 Phase transitions, 261, 1996. DOI: 10.1017/CBO9780511622564.
- [63] Tadatsugu Hoshino, Tetsuya Ishimaru, Hiroki Kawada, Iwao Ohdomari, Dominant Role of Corner Holes in the Decomposition Process of Silicon Islands on Si(111) Surfaces, *Jpn. J. Appl. Phys.* 38 (Part 1, No. 4A) (1999) 1858–1862, <https://doi.org/10.1143/JJAP.38.1858>.
- [64] K. Miyake, M. Ishida, K. Hata, H. Shigekawa, Role of corner holes in Si(111)-7 \times 7 structural formation studied by HBO_2 molecular irradiation and quenching, *Phys. Rev. B* 55 (1997) 5360, <https://doi.org/10.1103/PhysRevB.55.5360>.